



Detailed Properties of Equatorial Noise With Quasiperiodic Modulation

F. Němec, O. Santolik, M. Hayosh, F. Darrouzet, N. Cornilleau-Wehrin

► To cite this version:

F. Němec, O. Santolik, M. Hayosh, F. Darrouzet, N. Cornilleau-Wehrin. Detailed Properties of Equatorial Noise With Quasiperiodic Modulation. *Journal of Geophysical Research Space Physics*, 2018, 123 (7), pp.5344-5355. 10.1029/2018JA025382 . obspm-02296255

HAL Id: obspm-02296255

<https://hal-obspm.ccsd.cnrs.fr/obspm-02296255>

Submitted on 1 Nov 2021

HAL is a multi-disciplinary open access archive for the deposit and dissemination of scientific research documents, whether they are published or not. The documents may come from teaching and research institutions in France or abroad, or from public or private research centers.

L'archive ouverte pluridisciplinaire **HAL**, est destinée au dépôt et à la diffusion de documents scientifiques de niveau recherche, publiés ou non, émanant des établissements d'enseignement et de recherche français ou étrangers, des laboratoires publics ou privés.

Copyright

RESEARCH ARTICLE

10.1029/2018JA025382

Key Points:

- We analyze in detail 118 events using the times and frequencies of individual QP elements
- The modulation period of an event is usually quite stable, within about 25% from the median value
- Events with shorter modulation periods are typically more intense and have larger frequency drifts

Correspondence to:

 F. Němec,
frantisek.nemec@gmail.com

Citation:

Němec, F., Santolík, O., Hayosh, M., Darrouzet, F., & Cornilleau-Wehrin, N. (2018). Detailed properties of equatorial noise with quasiperiodic modulation. *Journal of Geophysical Research: Space Physics*, 123, 5344–5355. <https://doi.org/10.1029/2018JA025382>

Received 22 FEB 2018

Accepted 11 JUN 2018

Accepted article online 19 JUN 2018

Published online 6 JUL 2018

Detailed Properties of Equatorial Noise With Quasiperiodic Modulation

 F. Němec¹, O. Santolík^{1,2}, M. Hayosh², F. Darrouzet³, and N. Cornilleau-Wehrin^{4,5}

¹Faculty of Mathematics and Physics, Charles University, Prague, Czech Republic, ²Department of Space Physics, Institute of Atmospheric Physics, The Czech Academy of Sciences, Prague, Czech Republic, ³Royal Belgian Institute for Space Aeronomy, Brussels, Belgium, ⁴Laboratoire de Physique des Plasmas, Ecole Polytechnique, CNRS, Palaiseau, France, ⁵LESIA, Observatoire de Meudon, Meudon, France

Abstract Equatorial noise (EN) emissions are electromagnetic waves observed routinely in the equatorial region of the inner magnetosphere. Although they are typically continuous in time, they sometimes exhibit a quasiperiodic (QP) time modulation of the wave intensity, with modulation periods on the order of minutes. We perform a detailed analysis of 118 EN events with the QP modulation. The events are observed preferentially outside the plasmasphere. We determine the times and frequencies of individual QP elements forming the events. Apart from the event modulation period, this allows us to characterize the intensity and the frequency drift of individual QP wave elements. It is shown that the element intensity peaks at the magnetic equator. The modulation period within a single event is usually quite stable, with variations lower than 25% of the median value in the vast majority of cases. The events with shorter modulation periods are typically more intense, and they tend to have larger frequency drifts. These relations resemble the relations formerly revealed for extra low frequency/very low frequency quasiperiodic emissions, suggesting that the origin of the QP modulation of the wave intensity of EN and ELF/VLF emissions might be similar.

1. Introduction

Equatorial noise (EN) emissions (sometimes also termed *fast magnetosonic waves*) are whistler mode electromagnetic waves which are rather routinely observed in the vicinity of the geomagnetic equator both inside and outside the plasmasphere at radial distances between about 2 and 7 R_E (Boardsen et al., 2016; Kasahara et al., 1994; Laakso et al., 1990; Ma et al., 2013; Němec et al., 2005; Posch et al., 2015). They propagate with wave vectors oriented nearly perpendicular to the ambient magnetic field (Santolík et al., 2004; Walker, Balikhin, Shklyar, et al., 2015), that is, they are limited to frequencies below the lower hybrid frequency. They may be occasionally detected at altitudes as low as 700 km (Němec, Parrot, & Santolík, 2016; Santolík et al., 2016) and at radial distances as large as 10 R_E (Hrbáčková et al., 2015). Similar emissions off the geomagnetic equator were also reported (Tsurutani et al., 2014; Zhima et al., 2015). Although the emissions appeared as noise when they were observed for the first time in the low-resolution data (Russell et al., 1970), subsequent higher resolution data revealed that they were in fact formed by a system of harmonic spectral lines corresponding to the proton cyclotron frequency in the source region (Gurnett, 1976). The emissions are generated by ring-like proton distribution functions (Chen et al., 2011, 2016; Curtis & Wu, 1979; Liu et al., 2011; McClements & Dendy, 1993; McClements et al., 1994; Min & Liu, 2016; Sun et al., 2017) which were observed along with the event occurrence (Balikhin et al., 2015; Boardsen et al., 1992; Ma et al., 2014; Meredith et al., 2008; Perraut et al., 1982; Xiao et al., 2013; Xiao, Zhou, et al., 2015). It is noteworthy that the harmonic structure of the emissions is at times missing, resulting in a broadband spectra over a continuous frequency range (Chen et al., 2016; Tsurutani et al., 2014). This can be explained by the overlapping of adjacent unstable wave modes, as has been demonstrated both using linear theory (Sun et al., 2016a) and particle-in-cell simulations (Sun et al., 2016b). Although EN emissions stay confined to the equatorial plane, they may propagate in radial/azimuthal directions (Chen & Thorne, 2012; Horne et al., 2000; Němec, Santolík, Pickett, Hrbáčková, et al., 2013; Santolík et al., 2002; Xiao et al., 2012). EN is considered to be important for electron dynamics in the Van Allen radiation belts (Bortnik et al., 2015; Horne et al., 2007; Li et al., 2014; Ma et al., 2016; Ni et al., 2017; Shprits, 2016; Walker, Balikhin, Canu, et al., 2015), as well as for the formation of so-called butterfly distribution functions (Li, Bortnik, et al., 2016; Li, Ni, et al., 2016; Maldonado et al., 2016; Xiao, Yang, et al., 2015; Yang et al., 2017).

Although EN emissions were typically considered to be continuous in time, they sometimes exhibit a quasiperiodic (QP) time modulation of the wave intensity (Boardsen et al., 2014; Fu et al., 2014). This QP modulation of the EN wave intensity occurs in about 5% of the events, and it is statistically related to the periods of an increased solar wind speed (Němec, Santolík, Hrbáčková, et al., 2015). The events occur predominantly in the noon magnetic local time (MLT) sector. Although the occurrence rate of normal continuous EN also peaks close to the local noon (Hrbáčková et al., 2015), the noon peak of the occurrence rate of EN with the QP modulation of the wave intensity is much sharper, with the noontime occurrence rate about 4 times higher than the nighttime occurrence rate (Němec, Santolík, Hrbáčková, et al., 2015). Němec, Santolík, Hrbáčková, et al. (2015) further investigated high-resolution Cluster Wideband Data for all 17 events where these were available, and they revealed the presence of a harmonic line structure in all of them. The emissions may occasionally consist of two frequency bands of interleaved QP elements (Li et al., 2017) and were also observed at altitudes as low as 700 km (Parrot et al., 2016).

The origin of the QP modulation, however, remains unclear. A possibly similar phenomenon exhibiting a QP modulation of the wave intensity are extra low frequency/very low frequency (ELF/VLF) QP emissions (Cornilleau-Wehrlin et al., 1978; Sazhin & Hayakawa, 1994; Tixier & Cornilleau-Wehrlin, 1986), which also propagate in the whistler mode but approximately along the magnetic field lines (Hayosh et al., 2016; Němec, Santolík, Pickett, Parrot, et al., 2013). These are also observed primarily on the dayside (Engebretson et al., 2004; Morrison et al., 1994). Two main generation mechanisms were suggested to explain the formation of these events: (i) modulation of the source region by a compressional ultra low frequency wave (Chen, 1974; Kimura, 1974; Sato et al., 1974; Sazhin, 1987) and (ii) periodic wave generation based on a self-consistent modulation of magnetospheric flow cyclotron maser (Demekhov & Trakhtengerts, 1994; Pasmanik et al., 2004). However, a direct confirmation of any of these suggested generation mechanisms is still missing. We note that—albeit formed by individual elements drifting in frequency—the modulation periods of ELF/VLF QP emissions are generally much larger and their frequency sweep rates much lower than those of discrete chorus emissions (Gao et al., 2014a, 2014b), and they should not be confused.

We analyze detailed properties of 118 EN events with a QP modulation of the wave intensity observed by the Cluster spacecraft during the first 10 years of operation (2001–2010). We demonstrate that some of their properties are remarkably similar to the properties formerly reported for ELF/VLF QP emissions propagating nearly along the ambient magnetic field. The data set is described in section 2. The obtained results are presented in section 3, and they are discussed in section 4. Finally, section 5 contains a brief summary.

2. Data set

Electromagnetic wave data measured by the Cluster spacecraft are used in the present study. Cluster is a mission consisting of four satellites flying in a close constellation on nearly identical high inclination orbits. The orbital parameters evolved during the mission duration, but during the first years the spacecraft crossed the equatorial plane around their perigee at a radial distance of about $4 R_E$, optimal for EN observations. Multicomponent measurements of electromagnetic waves were performed by the Spatio-Temporal Analysis of Field Fluctuations Spectrum Analyzer (STAFF-SA). The instrument uses three orthogonal magnetic field components and two electric field components in the spin plane of the spacecraft to calculate onboard 5×5 spectral matrices in 27 frequency channels logarithmically spaced between 8 Hz and 4 kHz. The time resolution is 1 s for the power spectral densities (main diagonals of spectral matrices) and 4 s for phases and coherence (off-diagonal elements of spectral matrices). The measured data thus allow us to determine not only the intensity of observed electromagnetic waves but also their polarization and propagation properties. A more detailed description of the instrument was given by Cornilleau-Wehrlin et al. (1997, 2003). In addition to the electromagnetic wave measurements, the Waves of High frequency Sounder for Probing the Electron density by Relaxation instrument on board the Cluster spacecraft provides absolute measurements of the electron plasma number density in the range $0.2\text{--}80\text{ cm}^{-3}$ based on the resonance sounding technique (Décréau et al., 1997, 2001).

The data set analyzed in this paper consists of 118 events visually identified in total in the first 10 years of the Cluster spacecraft data (Němec, Santolík, Hrbáčková, et al., 2015). We note that if EN with a QP modulation of the wave intensity is observed at the same time by several Cluster spacecraft, it is counted as several separate events, one per spacecraft observing the emissions. An example of an EN event with a QP modulation of the wave intensity observed by Cluster 1 on 4 September 2001 between 08:37 UT and

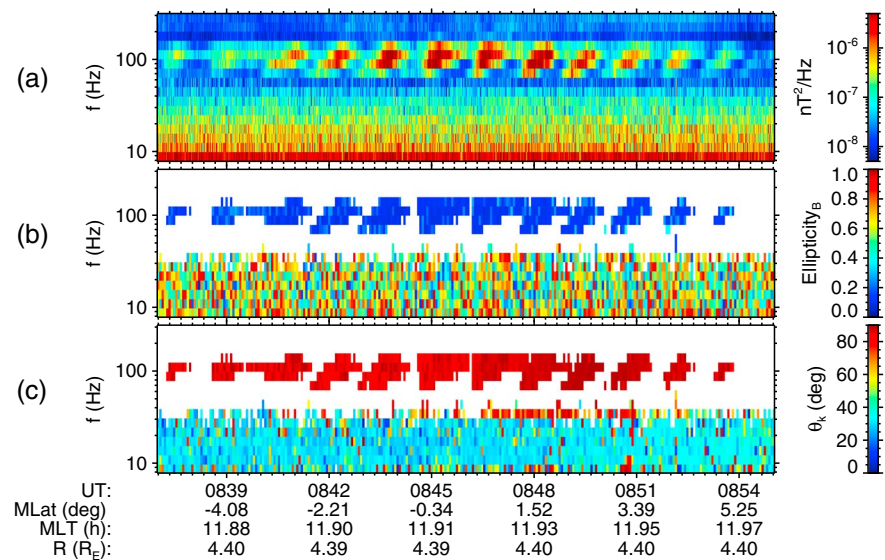


Figure 1. Example of an equatorial noise event with a quasiperiodic modulation of the wave intensity. The data were measured by Cluster 1 on 4 September 2001 between 08:37 UT and 08:55 UT. (a) Frequency-time spectrogram of power spectral density of magnetic field fluctuations. (b) Frequency-time plot of ellipticity of magnetic field fluctuations. (c) Frequency-time plot of wave normal angle. MLT = magnetic local time.

08:55 UT is shown in Figure 1. Figure 1a shows a frequency-time spectrogram of power spectral density of magnetic field fluctuations. EN is the intense emission at frequencies of about 100 Hz, which consists of several well-distinguishable QP elements. Considering that multicomponent magnetic field measurements are available, a detailed wave analysis can be done, as demonstrated in Figures 1b and 1c. This analysis was performed only for frequency-time intervals with power spectral density of magnetic field fluctuations larger than 10^{-7} nT² Hz⁻¹. Figure 1b shows a frequency-time plot of the ellipticity of magnetic field fluctuations (Santolík et al., 2003). The values of ellipticity correspond to the ratio of the middle and the largest axis of the polarization ellipsoid, and they may range between 0 and 1. The ellipticity of 0 corresponds to the linear polarization, while the ellipticity of 1 corresponds to the circular polarization. It can be seen that the EN emissions are nearly linearly polarized. The wave normal angle with respect to the ambient magnetic field shown in Figure 1c may range between 0° and 90°. The value of 0° corresponds to the wave vector oriented along/opposite the ambient magnetic field, while the value of 90° corresponds to the wave vector oriented perpendicular to the ambient magnetic field. It can be seen that the EN emissions propagate principally perpendicular to the ambient magnetic field.

In order to perform a detailed analysis of identified EN events with QP modulation, it is important to properly evaluate the timing of individual QP elements. In order to do so, we have developed a semiautomatic routine which allows us to identify individual intensity peaks at frequencies of interest. Given the limited frequency resolution of the STAFF-SA instrument (in the frequency range of interest about 10–50 Hz), it seems natural to perform the analysis in each STAFF-SA frequency band separately. The idea of the analysis is demonstrated in Figure 2. It shows exactly the same time interval as Figure 1, but this time we only show the power spectral density data in the STAFF-SA frequency bins where the EN event with the QP modulation was observed. Specifically, Figures 2a–2c show the time dependence of the power spectral density of magnetic field fluctuations in the frequency ranges 78–99, 99–125, and 125–157 Hz, respectively. The time variation exhibits several well-distinguishable peaks, corresponding to individual QP elements. In order to identify the beginning and ending times of the QP elements, we have used a procedure similar to the one used by Němec, Bezděková, et al. (2016), that is, we have identified the local minima in between the intensity peaks. These intensity minima are then considered to separate the consecutive peaks, that is, an intensity peak is considered to start just after the end of the preceding one. The identified intensity minima are shown by the red crosses in Figure 2. Such a peak identification was done for each of the 118 identified events, and for each of the relevant frequency ranges of the STAFF-SA instrument, resulting in total 320 analyzed time dependencies of power spectral density. Altogether, 3,474 intensity peaks were identified. The obtained results allow us to directly evaluate the frequencies, modulation periods, and intensities of the events.

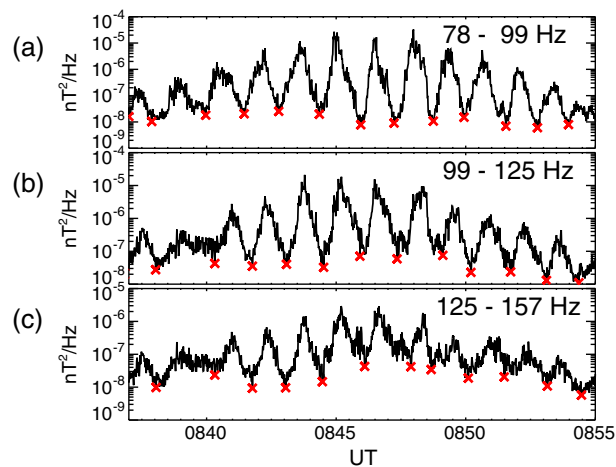


Figure 2. Time variation of the power spectral density of magnetic field fluctuations corresponding to the event from Figure 1 at various frequency ranges. (a) Frequency range 78–99 Hz, (b) frequency range 99–125 Hz, and (c) frequency range 125–157 Hz. The red crosses mark the beginning/ending times of individual quasiperiodic elements determined as the local intensity minima.

3. Results

In situ plasma density measurements performed by the Waves of High frequency Sounder for Probing the Electron density by Relaxation instrument at and around the times of the events allow us to identify plasmopause crossings (if present) and to evaluate whether the events were observed inside or outside the plasmasphere (Darrouzet et al., 2009, 2013). Given the Cluster polar orbit and the event occurrence close to the equatorial plane, a plasmopause crossing is generally observed only for events observed inside the plasmasphere. Event observations outside the plasmasphere effectively mean that the plasmasphere has a rather low radial extent. The Cluster spacecraft are then typically located outside the plasmasphere during the entire equatorial crossings, and no plasmopause crossings are observed. Out of the 118 analyzed events, 11 events were observed inside the plasmasphere, 12 events spanned both inside and outside the plasmasphere, and 78 events were observed outside the plasmasphere. No plasma density data were available, or the plasmopause was unclear in 17 events. With the given spacecraft orbit we have therefore collected more events outside the plasmasphere than inside the plasmasphere. Moreover, some events spanning both inside and outside the plasmasphere reveal a significant intensity decrease at the plasmopause when entering the plasmasphere. For example, the event reported by Němec, Santolík, Hrbáčková, et al. (2015) in their Figure 2, observed by Cluster 2 on 27 November 2003 between 02:24 UT and 03:16 UT, spanned both inside and outside the plasmasphere. However, there was a significant decrease of the event intensity at the time when the spacecraft was located inside the plasmasphere (approximately between 02:52 UT and 02:56 UT).

Figure 3a shows a histogram of frequencies where the individual events were observed. The binning on the abscissa corresponds to the frequency bins of the STAFF-SA instrument. The ordinate shows the number of events spanning over a given frequency bin. The error estimates (σ) were calculated separately in each frequency bin, assuming that the number of events in the bin (n) follows a Poisson distribution, that is, $\sigma = \sqrt{n}$. It can be seen that most events are observed at frequencies of about 100 Hz, with only a few at frequencies below 50 Hz/above 200 Hz. Considering that the events are generated at harmonics of the proton cyclotron frequency in the source region, it may be instructive to normalize the observed frequencies by the local proton cyclotron frequency. As the emissions may possibly propagate over a considerable radial distance (Horne et al., 2000; Santolík et al., 2002), using the proton cyclotron frequency at the observation point may be inappropriate in some events. However, it should still provide us with a rough estimate of harmonic numbers which are usually generated. The obtained results are shown in Figure 3b, which depicts the number of events observed at given normalized frequencies. Each event was considered to contribute to all normalized frequencies between the lowest and the largest normalized frequency of the event. Error estimates, calculated in the same way as in Figure 3a, are shown by the thinner gray curves. It can be seen that the normalized frequencies (harmonic numbers) are mostly between about 15 and 25.

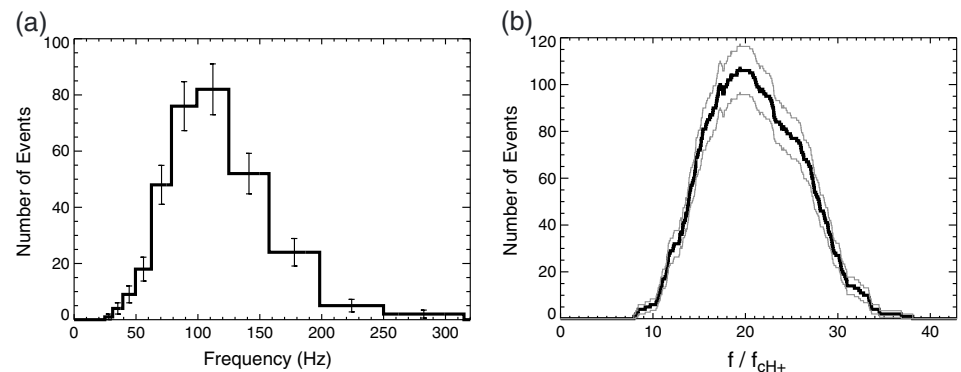


Figure 3. (a) Frequencies where the events are observed (118 events in total). The number of events spanning over a given frequency bin of the Spatio-Temporal Analysis of Field Fluctuations Spectrum Analyzer instrument is plotted. The error bars were calculated from the observed number of events assuming a Poisson distribution. (b) Same as (a) but for frequencies normalized by the proton cyclotron frequency at the observation point. Error estimates are marked by the thinner gray curves.

As for the intensity of the events, we can define an intensity of each QP element at a given frequency as an average power spectral density calculated over the time duration of the element. The QP element intensity is thus—as well as the beginning and ending times of individual QP elements—evaluated separately for each STAFF-SA frequency interval. As can be expected from the EN confinement to the vicinity of the equatorial plane (e.g., Němec et al., 2005), it is found that the main factor controlling the QP element intensity is the geomagnetic latitude. The obtained results are shown in Figure 4a. Each QP element intensity at each STAFF-SA frequency bin where it was observed is shown by a color point. The color corresponds to the respective frequency bin, following the color scale on the right-hand side. The color curves correspond to the best fit Gaussian dependencies in the frequency ranges 24.8–78.7, 78.7–157.5, and 157.5–315.0 Hz, respectively. These frequency ranges were selected to correspond to the STAFF-SA frequency intervals and to reasonably cover the entire frequency range of interest. It can be seen that the QP elements at lower frequencies are on average more intense and confined somewhat closer to the equatorial plane than QP elements at higher frequencies. Němec et al. (2006) reported that EN intensity tends to peak at the min-B equator, where the magnetic field magnitude along a given magnetic field line is minimal. The position of the min-B equator can be readily estimated by using, for example, Tsyganenko (1989) magnetospheric magnetic field model. Figure 4b demonstrates that the intensity of individual QP elements indeed peaks also at the min-B equator. Specifically, when the geomagnetic latitude is given with respect to the min-B equator in place of the dipole geomagnetic equator, the intensity dependencies get noticeably narrower and symmetric.

It is of interest to investigate how the modulation periods of the events evolve during the event duration or, in other words, how stable they are. Given that Cluster is a multispacecraft mission, with individual spacecraft typically following each other on rather similar orbits, a single EN emission is often observed by several

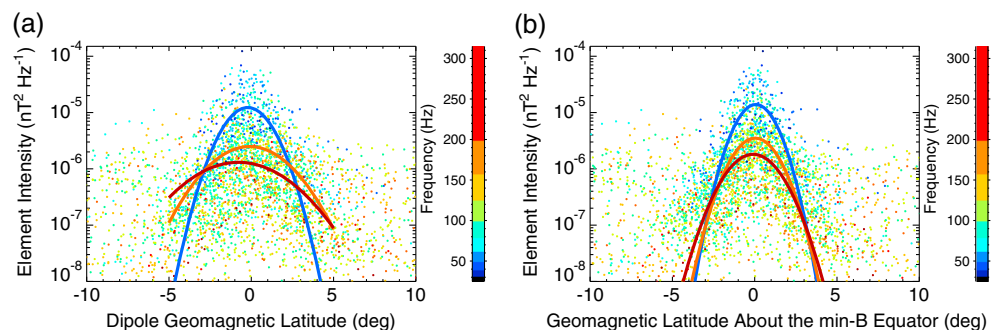


Figure 4. (a) Intensity of individual quasiperiodic elements as a function of the dipole geomagnetic latitude and frequency. The frequency is color coded according to the color scale on the right-hand side. The color curves correspond to the best fit Gaussian functions in the frequency ranges 24.8–78.7, 78.7–157.5, and 157.5–315.0 Hz, respectively. (b) Same as (a) but for the geomagnetic latitude relative to the min-B equator.

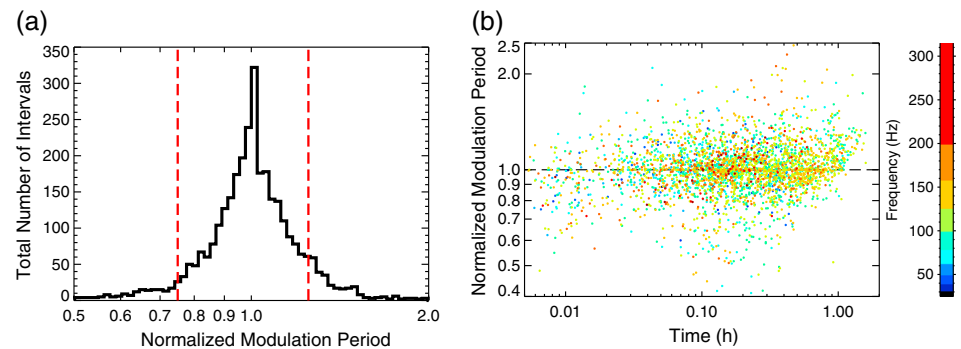


Figure 5. (a) Time separations between individual quasiperiodic elements of a given merged event normalized by the median of these time separations. The histogram is calculated using the data corresponding to all merged events and frequency ranges. The vertical red dashed lines correspond to $\pm 25\%$ interval. (b) Time separations between individual quasiperiodic elements normalized by the modulation periods of respective merged events as a function of time from the beginning of the merged events. The analysis was done separately for each frequency range, according to the color scale on the right-hand side.

spacecraft with a short time delay, as the spacecraft consecutively pass through the geomagnetic equator. Such an observation was evaluated as several (up to 4, depending on the number of Cluster spacecraft observing the emission) events in the aforementioned analysis. For the purpose of the analysis of the modulation period evolution, we, however, group all these consecutive observations together, resulting in a single merged event for each Cluster constellation pass through the equator. The total 118 EN events with the QP modulation of the wave intensity are thus grouped into 52 merged events. We note that the multispacecraft nature of the Cluster mission thus serves us here only to increase the total number of data and the time duration of individual events, with no analysis employing simultaneous multipoint measurements being involved. Figure 5a shows a histogram of normalized time differences between consecutive QP elements. It was calculated using the data corresponding to all merged events and STAFF-SA frequency intervals. For each merged event and STAFF-SA frequency interval, the time separations of consecutive QP elements were determined as the differences of the averages of element beginning and ending times. Finally, for each merged event and STAFF-SA frequency interval, these were normalized by the median of these time separations. The vertical red dashed lines show the 0.75 and 1.25 values, demonstrating that the time difference between consecutive QP elements is within 25% from the median modulation period in the vast majority of cases. Figure 5b shows the time evolution of the modulation periods. The normalized modulation periods from Figure 5a are plotted as a function of the time from the beginning of the merged event, that is, from the time when the first element forming the merged event was observed. The results are color coded as a function of the frequency, using the color scale on the right-hand side. Although the scatter of the data points is large, there appears to be a possible very weak increasing trend (Spearman rank correlation coefficient of about 0.15).

Hayosh et al. (2014) analyzed detailed properties of 2,264 ELF/VLF QP emissions propagating in the whistler mode approximately along the magnetic field lines identified in the electric field data measured by the low-altitude Detection of Electro-Magnetic Emissions Transmitted from Earthquake Regions (DEMETER) spacecraft. They showed that both the QP element intensity and the QP element frequency drift decrease as a function of the modulation period. We can investigate whether these relations are valid also for EN with the QP modulation, having identified the times of the EN QP elements (defined as the average of element beginning and ending times) at individual STAFF-SA frequency bins. This is done in Figures 6 and 7. Given the latitudinal dependence of the QP element intensity shown in Figure 4, we define the event intensity as the intensity of its most intense element. The modulation period of an event is defined, following Hayosh et al. (2014), as the median time difference between consecutive QP elements. The analysis is done separately for each of the three frequency ranges used in Figure 4. Figure 6a shows the intensities of individual events in the frequency range 24.8–78.7 Hz as a function of their modulation periods. The results are color coded as a function of the frequency, following the color scale on the right-hand side. The uncertainties of each of the data points are marked by the thin horizontal and vertical lines. The uncertainty σ_i of the maximum element intensity was estimated by considering the intensity difference ΔI between the most intense and the second most intense elements, that is, $\sigma_i = \Delta I / \sqrt{2}$. The uncertainty of the modulation period was calculated, separately for each event, from the distribution of time differences between consecutive QP elements.

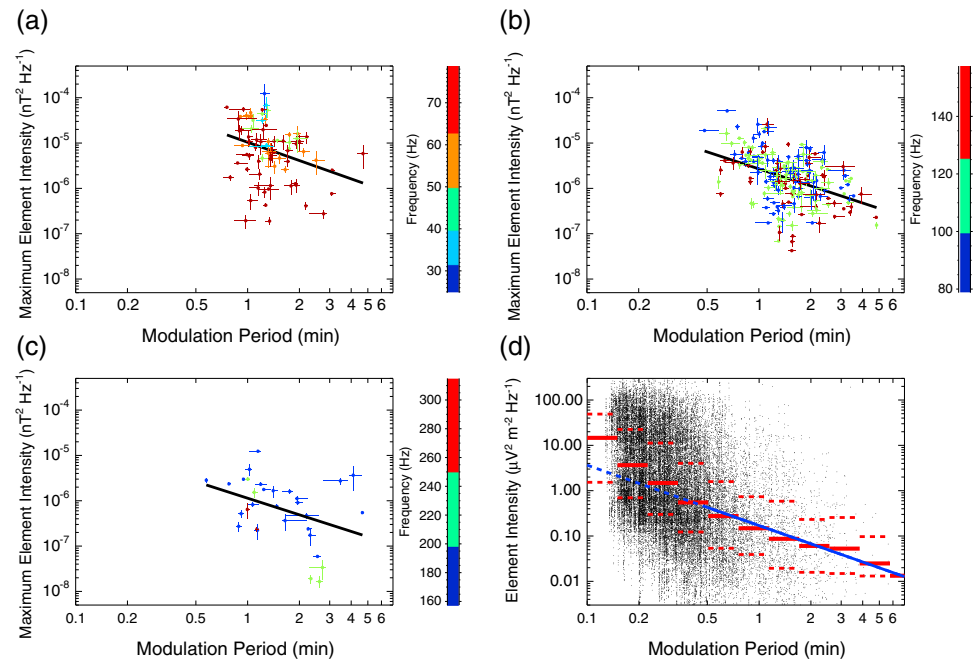


Figure 6. (a) Event intensity (defined as the maximum intensity of individual quasiperiodic elements) as a function of the event modulation period. The analysis was done separately for each frequency band of the Spatio-Temporal Analysis of Field Fluctuations Spectrum Analyzer instrument, according to the color scale on the right-hand side. The uncertainties of each of the data points are marked by the thin horizontal and vertical lines. The black line corresponds to the best power law fit in the frequency range 24.8–78.7 Hz. (b) The same as panel (a) but for the frequency range 78.7–157.5 Hz. (c) The same as panel (a) but for the frequency range 157.5–315.0 Hz. (d) Intensity of ELF/VLF quasiperiodic elements as a function of respective modulation periods as obtained by Hayosh et al. (2014). The solid horizontal red lines show the median values in individual modulation period intervals, and the dashed horizontal red lines show the respective 0.25 and 0.75 quartiles. The blue line corresponds to the best power law fit at modulation periods larger than 0.5 min.

We considered its 0.16 and 0.84 percentiles, which for a normal distribution correspond to ± 1 standard deviation ($T_{0.16}$ and $T_{0.84}$, respectively). The lower and upper estimates of the modulation period $T_{0.5}$ were then obtained as $T_{\text{low}} = T_{0.5} - (T_{0.5} - T_{0.16})/\sqrt{N}$ and $T_{\text{upp}} = T_{0.5} + (T_{0.84} - T_{0.5})/\sqrt{N}$, where N is the total number of QP elements identified in a given event. The solid black line in Figure 6a shows a power law fit ($y = Cx^a$). Figures 6b and 6c use the same format as Figure 6a, but they were obtained for frequency ranges 78.7–157.5 and 157.5–315.0 Hz, respectively. It can be seen that, consistently with the results from Figure 4, the events are less intense at higher frequencies. Moreover, a decreasing trend of the event intensity as a function of the modulation period is identified in all analyzed frequency ranges. For the purpose of the comparison, Figure 6d shows the results obtained by Hayosh et al. (2014) for ELF/VLF QP emissions. It uses the same range on the abscissa and the same logarithmic extent on the ordinate, that is, it allows for an easy visual comparison. The solid horizontal red lines show the median values in individual modulation period intervals, and the dashed horizontal red lines show the respective 0.25 and 0.75 quartiles. Additionally, the solid blue line shows the best power law fit at modulation periods larger than 0.5 min. This modulation period threshold was set somewhat arbitrarily, in order not to fit the more abruptly increasing intensities at very short modulation periods, which are not observed for EN (marked by the blue dashed line). Considering the large scatter of individual data points, the power law exponent of the best fit dependencies is remarkably similar. Specifically, the power law exponent of the blue line in Figure 6d is -1.33 ± 0.07 , and the power law exponents of the black lines in Figures 6a–6c are -1.34 ± 0.47 , -1.25 ± 0.19 , and -1.22 ± 0.54 , respectively. Note that the errors of power law exponents obtained for EN events with the QP modulation are larger than the errors of power law exponents obtained for ELF/VLF QP emissions due to the lower number of analyzed events.

Figure 7 deals with the frequency drift of the events. For each of the QP elements, the frequency drift is calculated using the time of the QP element at the minimum and maximum frequencies (the time of the QP element at a given frequency is defined as the time in the middle of the local minima preceding and following the element; the minimum and maximum frequencies are defined as central frequencies of the respective

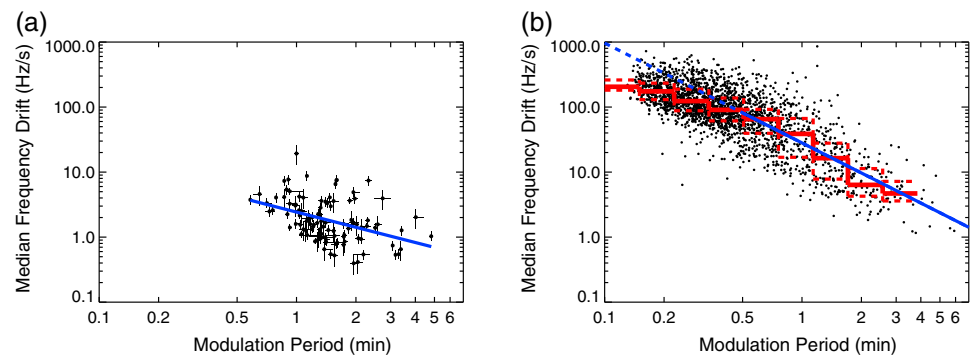


Figure 7. (a) Median frequency drifts of individual events as a function of their modulation periods. The uncertainties of individual data points are marked by thin horizontal and vertical lines. The blue line corresponds to the best power law fit. (b) Same as (a) but for ELF/VLF QP emissions analyzed by Hayosh et al. (2014). The red horizontal solid and dashed lines correspond to median and quartile values in individual modulation period intervals. The blue line corresponds to the best power law fit at modulation periods larger than 0.5 min.

STAFF-SA bins). Then, a median value of the frequency drifts of individual QP elements forming an event was used as a characteristic frequency drift of the event. The obtained results are shown in Figure 7a. We note that the determination of the frequency drifts is rather inaccurate due to the limited frequency resolution of the STAFF-SA instrument, in particular at higher frequencies and for events spanning over few STAFF-SA frequency bands. This was considered when calculating the uncertainties of individual data points, which are marked by the thin horizontal and vertical lines. The uncertainty of the modulation period was calculated in the same way as in Figure 6. The uncertainty of the frequency drift of a given event was obtained from the bandwidths of the lowest and highest frequency bands where the event was observed. The upper estimate of the frequency drift (i.e., the lower estimate of the event frequency extent) was obtained by assuming that the event spans over only one third of the frequency ranges of the appropriate lowest and highest frequency bands of the STAFF-SA instrument. Correspondingly, the lower estimate of the frequency drift (i.e., the upper estimate of the event frequency extent) was obtained by assuming that the event spans over two thirds of the appropriate lowest and highest frequency bands of the STAFF-SA instrument. Although the scatter of the individual data points is large, there is a clear systematic trend of the frequency drifts to decrease with increasing modulation period, as demonstrated by the best fit power law dependence shown by the blue line. Figure 7b shows the results obtained by Hayosh et al. (2014) for ELF/VLF QP emissions, using the same ranges on both abscissa and ordinate. The red horizontal solid and dashed lines again correspond to median and quartile values in individual modulation period intervals, and the solid blue line shows the best fit power law dependence at modulation periods larger than 0.5 min. It can be seen that the dependence obtained for EN events with the QP modulation is rather similar but decreasing somewhat slower. Specifically, while the power law exponent of the blue line in Figure 7a is about -0.78 ± 0.17 , the power law exponent of the blue line in Figure 7b is about -1.54 ± 0.05 . Again, due to the lower number of analyzed events, the errors of power law exponents obtained for EN events with the QP modulation are larger than the errors of power law exponents obtained for ELF/VLF QP emissions.

4. Discussion

Both the event observations primarily outside the plasmasphere and the intensity decrease at the plasma-pause observed for some events when entering the plasmasphere indicate that the events are generated outside the plasmasphere and they only occasionally propagate inside. Additionally, the frequencies where the events are observed typically range from about 13 to 30 $f_c H^+$. Considering that EN outside the plasmasphere is typically observed at higher harmonic frequencies than EN inside the plasmasphere (Boardsen et al., 2016; Němec, Santolík, Hrbáčková, & Cornilleau-Wehrin, 2015), these rather high harmonic numbers of EN with the QP modulation are also consistent with the events being generated primarily outside the plasmasphere. The characteristics of the 11 EN events with the QP modulation observed inside the plasmasphere and the 78 events observed outside the plasmasphere are rather similar, with no clear difference between the two groups of events. The events observed inside the plasmasphere have on average slightly lower frequencies, suggesting that they might have been generated in regions with larger plasma number densities (Chen et al., 2010; Ma et al., 2014). A possible generation of a small fraction of the events inside the plasmasphere thus

cannot be ruled out. We note that sporadic event observations well inside the plasmasphere are consistent with an analogous type of events observed at altitudes as low as 700 km (Parrot et al., 2016).

The events are limited to within few degrees from the geomagnetic equator, with the intensity peak just at the min-B equator. This is in agreement with the former results on all EN emissions (Němec et al., 2005, 2006). The observed larger latitudinal spread and lower intensity of the events at higher frequencies appear to be in agreement with the ray tracing calculation of event propagation, which shows that the emissions with lower frequencies tend to stay confined closer to the equatorial plane (Santolík et al., 2016). The calculated intensities of individual QP elements can be compared with former results obtained for normal continuous EN emissions. The median magnetic spectral power of EN in low-density regions (i.e., roughly outside the plasmasphere) and at latitudes within 5° from the geomagnetic equator was obtained by Boardsen et al. (2016) using Van Allen Probes measurements as a function of the radial distance and MLT (see their Figure 6c). The intensity distribution they obtained peaks at MLTs around noon, which is just the MLT sector where EN events with the QP modulation are usually observed, reaching values of about $2 \times 10^{-4} \text{ nT}^2 \text{ Hz}^{-1}$. These intensities are significantly larger than the intensities of EN with the QP modulation of the wave intensity obtained in the present paper, which are typically below $10^{-5} \text{ nT}^2 \text{ Hz}^{-1}$. This seems to be consistent with the finding that the intensity of EN with the QP modulation is larger for events with shorter modulation periods, considering that normal continuous EN might be possibly obtained as a limit of the QP-modulated EN when the modulation period goes to zero. This might be perhaps understood in terms of the generation region being close to an instability threshold, requiring always some time for the free energy to accumulate and the wave growth to occur, favoring possibly the generation mechanism based on an analogy with a self-consistent modulation of magnetospheric flow cyclotron maser (Demekhov & Trakhtengerts, 1994; Pasmanik et al., 2004).

The modulation period of a given event remains rather stable during the event duration. There appears to be a very weak trend for the modulation period to increase with time, but on the analyzed time scales (lower than 1 hr), the dependence is rather inconclusive. This might be vaguely consistent with the magnetospheric flow cyclotron maser theory suggested to explain ELF/VLF QP emissions (Demekhov & Trakhtengerts, 1994; Pasmanik et al., 2004), which predicts the modulation period to be inversely proportional to the flux of involved energetic particles. A possible decrease of the particle flux during the event duration would then result in the modulation period increase. The magnetospheric flow cyclotron maser theory appears to be further consistent with decreases of modulation periods of ELF/VLF QP emissions observed at the times of substorm injections (Manninen et al., 2013, 2014).

The analysis of detailed properties of EN with the QP modulation reveals some striking similarities with ELF/VLF QP emissions propagating in the whistler mode approximately along the magnetic field lines. We argue that the observed interrelations between event properties (modulation period, intensity, and frequency drift) are intrinsically related to the generation of emissions, being indicative of the generation mechanism and conditions in the source region. The similar dependencies obtained for EN with the QP modulation of the wave intensity and ELF/VLF QP emissions are then hardly a coincidence, but they may indicate that the origin of the QP modulation of the wave intensity (albeit unknown) might be the same for the two types emissions. We suggest that the observation of more intense events tending to have shorter modulation periods revealed by Hayosh et al. (2014) for ELF/VLF QP emissions and in the present paper for EN events with the QP modulation might be consistent with the aforementioned magnetospheric flow cyclotron maser.

5. Conclusions

We have analyzed 118 EN events with a QP modulation of the wave intensity observed by the Cluster spacecraft during the first 10 years of operation (2001–2010). We identified the times and frequencies of individual QP elements, which allowed us to determine the event modulation periods, intensities, and frequency drifts. Although the events occur preferentially outside the plasmasphere, some of them are observed well inside. The intensity of the QP elements generally peaks at the min-B equator, consistent with the event confinement to the vicinity of the equatorial plane. The modulation period within a single event is usually quite stable, within 25% of the median value in the vast majority of cases. It is found that the events with shorter modulation periods are typically more intense, and they tend to exhibit larger frequency drifts. These dependencies are similar to those reported by Hayosh et al. (2014) for ELF/VLF QP emissions propagating in the whistler mode nearly along the ambient magnetic field, possibly suggesting that the mechanism responsible for the origin of the QP modulation may also be similar for the two phenomena.

A further theoretical development is clearly needed in order to understand the origin of EN events with the QP modulation of the wave intensity. The detailed properties of the events determined in the present paper should, hopefully, help with this future work and limit the possibilities for the generation mechanisms considered when explaining this exciting phenomenon.

Acknowledgments

Cluster spacecraft data are accessible from the Cluster Science Archive (<https://www.cosmos.esa.int/web/csa/> access), and we would like to thank to all the involved personnel. The work of F. N. was supported by GACR grant 18-00844S. The work of O. S. was supported by MSMT grants LH 15304 and LTAUSA17070 and by the Praemium Academiae award from the CAS. The work of F. D. was supported by the ProDEX project (contract 13127/98/NL/VJ).

References

- Balikhin, M. A., Shprits, Y. Y., Walker, S. N., Chen, L., Cornilleau-Wehrin, N., Dandouras, I., et al. (2015). Observations of discrete harmonics emerging from equatorial noise. *Nature Communications*, 6, 7703. <https://doi.org/10.1038/ncomms8703>
- Boardsen, S. A., Gallagher, D. L., Gurnett, D. A., Peterson, W. K., & Green, J. L. (1992). Funnel-shaped, low-frequency equatorial waves. *Journal of Geophysical Research*, 97, 14,967–14,976. <https://doi.org/10.1029/92JA00827>
- Boardsen, S. A., Hospodarsky, G. B., Kletzing, C. A., Engebretson, M. J., Pfaff, R. F., Wygant, J. R., et al. (2016). Survey of the frequency dependent latitudinal distribution of the fast magnetosonic wave mode from Van Allen Probes Electric and Magnetic Field Instrument and Integrated Science waveform receiver plasma wave analysis. *Journal of Geophysical Research: Space Physics*, 121, 2902–2921. <https://doi.org/10.1002/2015JA021844>
- Boardsen, S. A., Hospodarsky, G. B., Kletzing, C. A., Pfaff, R. F., Kurth, W. S., Wygant, J. R., & MacDonald, E. A. (2014). Van Allen Probe observations of periodic rising frequencies of the fast magnetosonic mode. *Geophysical Research Letters*, 41, 8161–8168. <https://doi.org/10.1002/2014GL062020>
- Bortnik, J., Thorne, R. M., Ni, B., & Li, J. (2015). Analytical approximation of transit time scattering due to magnetosonic waves. *Geophysical Research Letters*, 42, 1318–1325. <https://doi.org/10.1002/2014GL062710>
- Chen, L. (1974). Theory of ULF modulation of VLF emissions. *Geophysical Research Letters*, 1(2), 73–75. <https://doi.org/10.1029/GL001i002p00073>
- Chen, L., Sun, J., Lu, Q., Gao, X., Xia, Z., & Zhima, Z. (2016). Generation of magnetosonic waves over a continuous spectrum. *Journal of Geophysical Research: Space Physics*, 121, 1137–1147. <https://doi.org/10.1002/2015JA022089>
- Chen, L., & Thorne, R. M. (2012). Perpendicular propagation of magnetosonic waves. *Geophysical Research Letters*, 39, L14102. <https://doi.org/10.1029/2012GL052485>
- Chen, L., Thorne, R. M., Jordanova, V. K., & Horne, R. B. (2010). Global simulation of magnetosonic wave instability in the storm time magnetosphere. *Journal of Geophysical Research*, 115, A11222. <https://doi.org/10.1029/2010JA015707>
- Chen, L., Thorne, R. M., Jordanova, V. K., Thomsen, M. F., & Horne, R. B. (2011). Magnetosonic wave instability analysis for proton ring distributions observed by the LANL magnetospheric plasma analyzer. *Journal of Geophysical Research*, 116, A03223. <https://doi.org/10.1029/2010JA016068>
- Cornilleau-Wehrin, N., Chanteur, G., Perraut, S., Rezeau, L., Robert, P., Roux, A., et al. (2003). First results obtained by the Cluster STAFF experiment. *Annals of Geophysics*, 21, 437–456. <https://doi.org/10.5194/angeo-21-437-2003>
- Cornilleau-Wehrin, N., Chauveau, P., Louis, S., Meyer, A., Nappa, J. M., Perraut, S., et al. (1997). The Cluster spatio-temporal analysis of field fluctuations (STAFF) experiment. *Space Science Reviews*, 79, 107–136. <https://doi.org/10.1023/A:1004979209565>
- Cornilleau-Wehrin, N., Gendrin, R., & Tixier, M. (1978). VLF waves: Conjugated ground-satellite relationships. *Space Science Reviews*, 22, 419–431. <https://doi.org/10.1007/BF00210877>
- Curtis, S. A., & Wu, C. S. (1979). Gyroharmonic emissions induced by energetic ions in the equatorial plasmasphere. *Journal of Geophysical Research*, 84(A6), 2597–2607. <https://doi.org/10.1029/JA084iA06p02597>
- Darrrouzet, F., Gallagher, D. L., André, N., Carpenter, D. L., Dandouras, I., Décréau, P. M. E., et al. (2009). Plasmaspheric density structures and dynamics: Properties observed by the CLUSTER and IMAGE missions. *Space Science Reviews*, 145(1–2), 55–106. <https://doi.org/10.1007/s11214-008-9438-9>
- Darrrouzet, F., Pierrard, V., Benck, S., Lointier, G., Cabrera, J., Borremans, K., et al. (2013). Links between the plasmopause and the radiation belt boundaries as observed by the instruments CIS, RAPID, and WHISPER onboard Cluster. *Journal of Geophysical Research: Space Physics*, 118, 4176–4188. <https://doi.org/10.1002/jgra.50239>
- Décréau, P. M. E., Ferreau, P., Krasnoselskikh, V., Guirriec, E. L., Lévêque, M., Martin, P., et al. (2001). Early results from the Whisper instrument on Cluster: An overview. *Annals of Geophysics*, 19, 1241–1258. <https://doi.org/10.5194/angeo-19-1241-2001>
- Décréau, P. M. E., Ferreau, P., Krasnoselskikh, V., Lévêque, M., Martin, P., Randriamboarison, O., et al. (1997). WHISPER, a resonance sounder and wave analyser: Performances and perspectives for the Cluster mission. *Space Science Reviews*, 79(1–2), 157–193. <https://doi.org/10.1023/A:1004931326404>
- Demekhov, A. G., & Trakhtengerts, V. Y. (1994). A mechanism of formation of pulsating aurorae. *Journal of Geophysical Research*, 99(A4), 5831–5841. <https://doi.org/10.1029/93JA01804>
- Engebretson, M. J., Posch, J. L., Halford, A. J., Shelburne, G. A., Smith, A. J., Spasojević, M., et al. (2004). Latitudinal and seasonal variations of quasiperiodic and periodic VLF emissions in the outer magnetosphere. *Journal of Geophysical Research*, 109, A05216. <https://doi.org/10.1029/2003JA010335>
- Fu, H. S., Cao, J. B., Zhima, Z., Khotyaintsev, Y. V., Angelopoulos, V., Santolík, O., et al. (2014). First observation of rising-tone magnetosonic waves. *Geophysical Research Letters*, 41, 7419–7426. <https://doi.org/10.1002/2014GL061867>
- Gao, X., Li, W., Thorne, R. M., Bortnik, J., Angelopoulos, V., Lu, Q., et al. (2014a). New evidence for generation mechanisms of discrete and hiss-like whistler mode waves. *Geophysical Research Letters*, 41, 4805–4811. <https://doi.org/10.1002/2014GL060707>
- Gao, X., Li, W., Thorne, R. M., Bortnik, J., Angelopoulos, V., Lu, Q., et al. (2014b). Statistical results describing the bandwidth and coherence coefficient of whistler mode waves using THEMIS waveform data. *Journal of Geophysical Research: Space Physics*, 119, 8992–9003. <https://doi.org/10.1002/2014JA020158>
- Gurnett, D. A. (1976). Plasma wave interactions with energetic ions near the magnetic equator. *Journal of Geophysical Research*, 81, 2765–2770. <https://doi.org/10.1029/JA081i016p02765>
- Hayosh, M., Němec, F., Santolík, O., & Parrot, M. (2014). Statistical investigation of VLF quasiperiodic emissions measured by the DEMETER spacecraft. *Journal of Geophysical Research: Space Physics*, 119. <https://doi.org/10.1002/2013JA019731>
- Hayosh, M., Němec, F., Santolík, O., & Parrot, M. (2016). Propagation properties of quasiperiodic VLF emissions observed by the DEMETER spacecraft. *Geophysical Research Letters*, 43, 1007–1014. <https://doi.org/10.1002/2015GL067373>
- Horne, R. B., Thorne, R. M., Glauert, S. A., Meredith, N. P., Pokhotelov, D., & Santolík, O. (2007). Electron acceleration in the Van Allen radiation belts by fast magnetosonic waves. *Geophysical Research Letters*, 34, L17107. <https://doi.org/10.1029/2007GL030267>
- Horne, R. B., Wheeler, G. V., & Alleyne, H. S. C. K. (2000). Proton and electron heating by radially propagating fast magnetosonic waves. *Journal of Geophysical Research*, 105(A12), 27,597–27,610. <https://doi.org/10.1029/2000JA000018>

- Hrbáčková, Z., Santolík, O., Němec, F., Macúšová, E., & Cornilleau-Wehrin, N. (2015). Systematic analysis of occurrence of equatorial noise emissions using 10 years of data from the Cluster mission. *Journal of Geophysical Research: Space Physics*, 120, 1007–1021. <https://doi.org/10.1002/2014JA020268>
- Kasahara, Y., Kenmochi, H., & Kimura, I. (1994). Propagation characteristics of the ELF emissions observed by the satellite Akebono in the magnetic equatorial plane. *Radio Science*, 29, 751–767. <https://doi.org/10.1029/94RS00445>
- Kimura, I. (1974). Interrelation between VLF and ULF emissions. *Space Science Reviews*, 16, 389–411. <https://doi.org/10.1007/BF00171565>
- Laakso, H., Junginger, H., Roux, A., Schmidt, R., & de Villedary, C. (1990). Magnetosonic waves above f_{CH+} at geostationary orbit: GEOS 2 results. *Journal of Geophysical Research*, 95, 10,609–10,621. <https://doi.org/10.1029/JA095iA07p10609>
- Li, J., Bortnik, J., Li, W., Ma, Q., Thorne, R. M., Kletzing, C. A., et al. (2017). Interactions between magnetosonic waves and radiation belt electrons: Comparisons of quasi-linear calculations with test particle simulations. *Journal of Geophysical Research: Space Physics*, 122, 1600–1610. <https://doi.org/10.1002/2016JA023536>
- Li, J., Bortnik, J., Thorne, R. M., Li, W., Ma, Q., Baker, D. N., et al. (2016). Ultrarelativistic electron butterfly distributions created by parallel acceleration due to magnetosonic waves. *Journal of Geophysical Research: Space Physics*, 121, 3212–3222. <https://doi.org/10.1002/2016JA022370>
- Li, J., Ni, B., Ma, Q., Xie, L., Pu, Z., Fu, S., et al. (2016). Formation of energetic electron butterfly distributions by magnetosonic waves via Landau resonance. *Geophysical Research Letters*, 43, 3009–3016. <https://doi.org/10.1002/2016GL067853>
- Li, J., Ni, B., Xie, L., Pu, Z., Bortnik, J., Thorne, R. M., et al. (2014). Interactions between magnetosonic waves and radiation belt electrons: Comparisons of quasi-linear calculations with test particle simulations. *Geophysical Research Letters*, 41, 4828–4834. <https://doi.org/10.1002/2014GL060461>
- Liu, K., Gary, S. P., & Winske, D. (2011). Excitation of magnetosonic waves in the terrestrial magnetosphere: Particle-in-cell simulations. *Journal of Geophysical Research*, 116, A07212. <https://doi.org/10.1029/2010JA016372>
- Ma, Q., Li, W., Chen, L., Thorne, R. M., & Angelopoulos, V. (2014). Magnetosonic wave excitation by ion ring distributions in the Earth's inner magnetosphere. *Journal of Geophysical Research: Space Physics*, 119, 844–852. <https://doi.org/10.1002/2013JA019591>
- Ma, Q., Li, W., Thorne, R. M., & Angelopoulos, V. (2013). Global distribution of equatorial magnetosonic waves observed by THEMIS. *Geophysical Research Letters*, 40, 1895–1901. <https://doi.org/10.1002/grl.50434>
- Ma, Q., Li, W., Thorne, R. M., Bortnik, J., Kletzing, C. A., Kurth, W. S., & Hospodarsky, G. B. (2016). Electron scattering by magnetosonic waves in the inner magnetosphere. *Journal of Geophysical Research: Space Physics*, 121, 274–285. <https://doi.org/10.1002/2015JA021992>
- Maldonado, A. A., Chen, L., Claudepierre, S. G., Bortnik, J., Thorne, R. M., & Spence, H. (2016). Electron butterfly distribution modulation by magnetosonic waves. *Geophysical Research Letters*, 43, 3051–3059. <https://doi.org/10.1002/2016GL068161>
- Manninen, J., Demekhov, A. G., Titova, E. E., Kozlovsky, A. E., & Pasmanik, D. L. (2014). Quasiperiodic VLF emissions with short-period modulation and their relationship to whistlers: A case study. *Journal of Geophysical Research: Space Physics*, 119, 3544–3557. <https://doi.org/10.1002/2013JA019743>
- Manninen, J., Kleimova, N. G., Kozyreva, O. V., Bessalov, P. A., & Kozlovsky, A. E. (2013). Non-typical ground-based quasi-periodic VLF emissions observed at $L \sim 5.3$ under quiet geomagnetic conditions at night. *Journal of Atmospheric and Solar-Terrestrial Physics*, 99, 123–128. <https://doi.org/10.1016/j.jastp.2012.05.007>
- McClements, K. G., & Dendy, R. O. (1993). Ion cyclotron harmonic wave generation by ring protons in space plasmas. *Journal of Geophysical Research*, 98, 11,689–11,700. <https://doi.org/10.1029/93JA00158>
- McClements, K. G., Dendy, R. O., & Lashmore-Davis, C. N. (1994). A model for the generation of obliquely propagating ULF waves near the magnetic equator. *Journal of Geophysical Research*, 99, 23,685–23,693. <https://doi.org/10.1029/94JA01979>
- Meredith, N. P., Horne, R. B., & Anderson, R. R. (2008). Survey of magnetosonic waves and proton ring distributions in the Earth's inner magnetosphere. *Journal of Geophysical Research*, 113, A06213. <https://doi.org/10.1029/2007JA012975>
- Min, K., & Liu, K. (2016). Understanding the growth rate patterns of ion Bernstein instabilities by ring-like proton velocity distributions. *Journal of Geophysical Research: Space Physics*, 121, 3036–3049. <https://doi.org/10.1002/2016JA022524>
- Morrison, K., Engebretson, M. J., Beck, J. R., Johnson, J. E., Arnoldy, R. L., Cahill, J. L. J., et al. (1994). A study of quasi-periodic ELF-VLF emissions at three antarctic stations: Evidence for off-equatorial generation? *Annals of Geophysics*, 12, 139–146. <https://doi.org/10.1007/s00585-994-0139-8>
- Němec, F., Bezděková, B., Manninen, J., Parrot, M., Santolík, O., Hayosh, M., & Turunen, T. (2016). Conjugate observations of a remarkable quasiperiodic event by the low-altitude DEMETER spacecraft and ground-based instruments. *Journal of Geophysical Research: Space Physics*, 121, 8790–8803. <https://doi.org/10.1002/2016JA022968>
- Němec, F., Parrot, M., & Santolík, O. (2016). Equatorial noise emissions observed by the DEMETER spacecraft during geomagnetic storms. *Journal of Geophysical Research: Space Physics*, 121, 9744–9757. <https://doi.org/10.1002/2016JA023145>
- Němec, F., Santolík, O., Gereová, K., Macúšová, E., de Conchy, Y., & Cornilleau-Wehrin, N. (2005). Initial results of a survey of equatorial noise emissions observed by the Cluster spacecraft. *Planetary and Space Science*, 53, 291–298. <https://doi.org/10.1016/j.pss.2004.09.055>
- Němec, F., Santolík, O., Gereová, K., Macúšová, E., Laakso, H., de Conchy, Y., et al. (2006). Equatorial noise: Statistical study of its localization and the derived number density. *Advances in Space Research*, 37, 610–616. <https://doi.org/10.1016/j.asr.2005.03.025>
- Němec, F., Santolík, O., Hrbáčková, Z., & Cornilleau-Wehrin, N. (2015). Intensities and spatiotemporal variability of equatorial noise emissions observed by the Cluster spacecraft. *Journal of Geophysical Research: Space Physics*, 120, 1620–1632. <https://doi.org/10.1002/2014JA020814>
- Němec, F., Santolík, O., Hrbáčková, Z., Pickett, J. S., & Cornilleau-Wehrin, N. (2015). Equatorial noise emissions with quasiperiodic modulation of wave intensity. *Journal of Geophysical Research: Space Physics*, 120, 2649–2661. <https://doi.org/10.1002/2014JA020816>
- Němec, F., Santolík, O., Pickett, J. S., Hrbáčková, Z., & Cornilleau-Wehrin, N. (2013). Azimuthal directions of equatorial noise propagation determined using 10 years of data from the Cluster spacecraft. *Journal of Geophysical Research: Space Physics*, 118, 7160–7169. <https://doi.org/10.1002/2013JA019373>
- Němec, F., Santolík, O., Pickett, J. S., Parrot, M., & Cornilleau-Wehrin, N. (2013). Quasiperiodic emissions observed by the Cluster spacecraft and their association with ULF magnetic pulsations. *Journal of Geophysical Research: Space Physics*, 118, 4210–4220. <https://doi.org/10.1002/jgra.50406>
- Ni, B., Hua, M., Zhou, R., Yi, J., & Fu, S. (2017). Competition between outer zone electron scattering by plasmaspheric hiss and magnetosonic waves. *Geophysical Research Letters*, 44, 3465–3474. <https://doi.org/10.1002/2017GL072989>
- Parrot, M., Němec, F., Santolík, O., & Cornilleau-Wehrin, N. (2016). Equatorial noise emissions with a quasiperiodic modulation observed by DEMETER at harmonics of the O^+ ion gyrofrequency. *Journal of Geophysical Research: Space Physics*, 121, 10,289–10,302. <https://doi.org/10.1002/2016JA022989>
- Pasmanik, D. L., Demekhov, A. G., Trakhtengerts, V. Y., & Parrot, M. (2004). Modeling whistler wave generation regimes in magnetospheric cyclotron maser. *Annals of Geophysics*, 22, 3561–3570. <https://doi.org/10.5194/angeo-22-3561-2004>

- Perraut, S., Roux, A., Robert, P., Gendrin, R., Sauvaud, J. A., Bosqued, J. M., et al. (1982). A systematic study of ULF waves above f_{H+} from GEOS 1 and 2 measurements and their relationships with proton ring distributions. *Journal of Geophysical Research*, 87, 6219–6236. <https://doi.org/10.1029/JA087iA08p06219>
- Posch, J. L., Engebretson, M. J., Olson, C. N., Thaller, S. A., Breneman, A. W., Wygant, J. R., et al. (2015). Low-harmonic magnetosonic waves observed by the Van Allen Probes. *Journal of Geophysical Research: Space Physics*, 120, 6230–6257. <https://doi.org/10.1002/2015JA021179>
- Russell, C. T., Holzer, R. E., & Smith, E. J. (1970).OGO 3 observations of ELF noise in the magnetosphere. The nature of the equatorial noise. *Journal of Geophysical Research*, 75(4), 755–768. <https://doi.org/10.1029/JA075i004p00755>
- Santolik, O., Némec, F., Gereová, K., Macúšová, E., de Conchy, Y., & Cornilleau-Wehrin, N. (2004). Systematic analysis of equatorial noise below the lower hybrid frequency. *Annals of Geophysics*, 22, 2587–2595. <https://doi.org/10.5194/angeo-22-2587-2004>
- Santolik, O., Parrot, M., & Lefeuvre, F. (2003). Singular value decomposition methods for wave propagation analysis. *Radio Science*, 38(1), 1010. <https://doi.org/10.1029/2000RS002523>
- Santolik, O., Parrot, M., & Némec, F. (2016). Propagation of equatorial noise to low altitudes: Decoupling from the magnetosonic mode. *Geophysical Research Letters*, 43, 6694–6704. <https://doi.org/10.1002/2016GL069582>
- Santolik, O., Pickett, J. S., Gurnett, D. A., Maksimovic, M., & Cornilleau-Wehrin, N. (2002). Spatiotemporal variability and propagation of equatorial noise observed by Cluster. *Journal of Geophysical Research*, 107(A12), 1495. <https://doi.org/10.1029/2001JA009159>
- Sato, N., Hayashi, K., Kokubun, S., Oguti, T., & Fukunishi, H. (1974). Relationships between quasi-periodic VLF emission and geomagnetic pulsation. *Journal of Atmospheric and Terrestrial Physics*, 36, 1515–1526. [https://doi.org/10.1016/0021-9169\(74\)90229-3](https://doi.org/10.1016/0021-9169(74)90229-3)
- Sazhin, S. S. (1987). An analytical model of quasiperiodic ELF-VLF emissions. *Planetary and Space Science*, 35(10), 1267–1274. [https://doi.org/10.1016/0032-0633\(87\)90111-5](https://doi.org/10.1016/0032-0633(87)90111-5)
- Sazhin, S. S., & Hayakawa, M. (1994). Periodic and quasiperiodic VLF emissions. *Journal of Geophysical Research*, 99, 735–753. [https://doi.org/10.1016/0021-9169\(94\)90130-9](https://doi.org/10.1016/0021-9169(94)90130-9)
- Shprits, Y. Y. (2016). Estimation of bounce resonant scattering by fast magnetosonic waves. *Geophysical Research Letters*, 43, 998–1006. <https://doi.org/10.1002/2015GL066796>
- Sun, J., Gao, X., Chen, L., Lu, Q., Tao, X., & Wang, S. (2016a). A parametric study for the generation of ion Bernstein modes from a discrete spectrum to a continuous one in the inner magnetosphere. I. Linear theory. *Physics of Plasmas*, 23, 022901. <https://doi.org/10.1063/1.4941283>
- Sun, J., Gao, X., Lu, Q., Chen, L., Liu, X., Wang, X., et al. (2017). Spectral properties and associated plasma energization by magnetosonic waves in the Earth's magnetosphere: Particle-in-cell simulations. *Journal of Geophysical Research: Space Physics*, 122, 5377–5390. <https://doi.org/10.1002/2017JA024027>
- Sun, J., Gao, X., Lu, Q., Chen, L., Tao, X., & Wang, S. (2016b). A parametric study for the generation of ion Bernstein modes from a discrete spectrum to a continuous one in the inner magnetosphere. II. Particle-in-cell simulations. *Physics of Plasmas*, 23, 022902. <https://doi.org/10.1063/1.4941284>
- Tixier, M., & Cornilleau-Wehrin, N. (1986). How are the VLF quasi-periodic emissions controlled by harmonics of field line oscillations? The results of a comparison between ground and GEOS satellites measurements. *Journal of Geophysical Research*, 91(A6), 6899–6919. <https://doi.org/10.1029/JA091iA06p06899>
- Tsurutani, B., Falkowski, B. J., Pickett, J. S., Verkhoglyadova, O. P., Santolik, O., & Lakhina, G. S. (2014). Extremely intense ELF magnetosonic waves: A survey of polar observations. *Journal of Geophysical Research: Space Physics*, 119, 964–977. <https://doi.org/10.1002/2013JA019284>
- Tsyganenko, N. A. (1989). A magnetospheric magnetic field model with a warped tail current sheet. *Planetary and Space Science*, 37, 5–20. [https://doi.org/10.1016/0032-0633\(89\)90066-4](https://doi.org/10.1016/0032-0633(89)90066-4)
- Walker, S. N., Balikhin, M. A., Canu, P., Cornilleau-Wehrin, N., & Moiseenko, I. (2015). Investigation of the Chirikov resonance overlap criteria for equatorial magnetosonic waves. *Journal of Geophysical Research: Space Physics*, 120, 8774–8781. <https://doi.org/10.1002/2015JA021718>
- Walker, S. N., Balikhin, M. A., Shklyar, D. R., Yearby, K. H., Canu, P., Carr, C. M., & Dandouras, I. (2015). Experimental determination of the dispersion relation of magnetosonic waves. *Journal of Geophysical Research: Space Physics*, 120, 9632–9650. <https://doi.org/10.1002/2015JA021746>
- Xiao, F., Yang, C., Su, Z., Zhou, Q., He, Z., He, Y., et al. (2015). Wave-driven butterfly distribution of Van Allen belt relativistic electrons. *Nature Communications*, 6, 8590. <https://doi.org/10.1038/ncomms9590>
- Xiao, F., Zhou, Q., He, Z., & Tang, L. (2012). Three-dimensional ray tracing of fast magnetosonic waves. *Journal of Geophysical Research*, 117, A06208. <https://doi.org/10.1029/2012JA017589>
- Xiao, F., Zhou, Q., He, Z., Yang, C., He, Y., & Tang, L. (2013). Magnetosonic wave instability by proton ring distributions: Simultaneous data and modeling. *Journal of Geophysical Research: Space Physics*, 118, 4053–4058. <https://doi.org/10.1002/jgra.50401>
- Xiao, F., Zhou, Q., He, Y., Yang, C., Liu, S., Baker, D. N., et al. (2015). Penetration of magnetosonic waves into the plasmasphere observed by the Van Allen Probes. *Geophysical Research Letters*, 42, 7287–7294. <https://doi.org/10.1002/2015GL065745>
- Yang, C., Su, Z., Xiao, F., Zheng, H., Wang, Y., Wang, S., et al. (2017). A positive correlation between energetic electron butterfly distributions and magnetosonic waves in the radiation belt slot region. *Geophysical Research Letters*, 44, 3980–3990. <https://doi.org/10.1002/2017GL073116>
- Zhima, Z., Chen, L., Fu, H., Cao, J., Horne, R. B., & Reeves, G. (2015). Observations of discrete magnetosonic waves off the magnetic equator. *Geophysical Research Letters*, 42, 9694–9701. <https://doi.org/10.1002/2015GL066255>